

AttnRegDeepLab: A Two-Stage Decoupled Framework for Interpretable Embryo Fragmentation Grading

Ming-Jhe Lee

Department of Electrical Engineering
National Taiwan Ocean University
Keelung 202301, Taiwan
jerry80098009@gmail.com

Ming-Jer Chen

Department of Obstetrics, Gynecology
and Woman's Health, TVGH, 407219
Taichung, Taiwan
mingjerchen@gmail.com

Chang-Hong Wu

Department of Electrical Engineering
National Taiwan Ocean University
Keelung 202301, Taiwan
s0979979782@gmail.com

Jung-Hua Wang*

AI Research Center
National Taiwan Ocean University
Keelung 202301
jhwang@email.ntou.edu.tw

Yu-Chiao Yi

Department of Obstetrics, Gynecology
and Woman's Health, TVGH, 407219
Taichung, Taiwan
yuchiaoyi@gmail.com

Tsung-Hsien Lee

Department of Obstetrics and
Gynecology, CSMU Hospital,
Taichung 40201, Taiwan
jackth.lee@gmail.com

Abstract—Embryo fragmentation is a morphological indicator critical for evaluating developmental potential in In Vitro Fertilization (IVF). However, manual grading is subjective and inefficient, while existing deep learning solutions often lack clinical explainability or suffer from accumulated errors in segmentation area estimation. To address these issues, this study proposes AttnRegDeepLab (Attention-Guided Regression DeepLab), a framework characterized by dual-branch Multi-Task Learning (MTL). A vanilla DeepLabV3+ decoder is modified by integrating Attention Gates into its skip connections, explicitly suppressing cytoplasmic noise to preserve contour details. Furthermore, a Multi-Scale Regression Head is introduced with a Feature Injection mechanism to propagate global grading priors into the segmentation task, rectifying systematic quantification errors. A 2-stage decoupled training strategy is proposed to address the gradient conflict in MTL. Also, a *range-based loss* is designed to leverage weakly labeled data. Our method achieves robust grading precision while maintaining excellent segmentation accuracy (Dice coefficient =0.729), in contrast to the end-to-end counterpart that might minimize grading error at the expense of contour integrity. This work provides a clinically interpretable solution that balances visual fidelity and quantitative precision.

Keywords: Embryo Grading, Multi-Task Learning, Explainable AI, Gradient Conflict, Semantic Segmentation, Decoupled Training.

I. INTRODUCTION

A. Background

Infertility represents a formidable global public health concern, with Assisted Reproductive Technology (ART), particularly In Vitro Fertilization (IVF), established as the cornerstone clinical intervention. The ultimate success of an IVF treatment cycle hinges critically on the outcome of the embryo transfer procedure, which is, in turn, highly dependent on the morphological quality of the transferred embryo [1]. Within the constellation of indicators used for embryo assessment, embryo fragmentation is widely recognized as a profound negative prognostic factor. Defined as the generation and presence of anucleate cytoplasmic fragments during the early cleavage stages of cell division, fragmentation

significantly compromises the intrinsic developmental potential of the embryo and, consequently, diminishes subsequent implantation rates [2]. Quantitative and qualitative assessments of this specific morphological characteristic are therefore essential for optimizing embryo selection and maximizing ART efficacy.

Current clinical practice widely adopts the Gardner grading system or comparable standards, which typically categorize the degree of fragmentation into discrete grades: Grade A (<10%), Grade B (10–25%), Grade C (25–50%), and Grade D (>50%). However, such manual assessment is inherently subjective and heavily reliant on the experience of the embryologist. Studies indicate that even among senior practitioners, significant inter-observer variability exists regarding the estimation of fragmentation proportions [3], [4]. This subjectivity poses a risk of misclassifying viable embryos, thereby adversely affecting transfer decisions and clinical outcomes.

B. Motivation and Technical Challenges

To mitigate the limitations of manual assessment, Computer-Aided Diagnosis (CAD) systems have been developed. Nevertheless, existing automated solutions encounter significant technical bottlenecks in clinical deployment. First, early texture analysis methods (e.g., GLCM) lack sufficient feature discriminability when processing complex embryonic cytoplasmic textures, struggling to distinguish between pathological fragments and normal cellular structures. Second, while deep learning-based pure regression models can predict grades, they suffer from the black box issue; they fail to provide visual evidence of fragment localization, thus falling short of the stringent explainability requirements in medical AI.

To enhance interpretability, an ideal system should simultaneously output both a quantitative grade and a segmentation mask. However, these tasks present an inherent optimization conflict: segmentation prioritizes pixel-level boundary fidelity, whereas grading focuses on global area estimation. In a shared backbone network, this conflict frequently induces the negative transfer problem [5], [6], where the convergence of one task is compromised to accommodate the other. This remains a primary obstacle in multi-task learning for medical imaging applications. To address these challenges, this paper proposes an integrated framework designed for precise fragmentation analysis.

C. Contributions

The primary contributions of this work are threefold. First, we introduce an integrated framework that leverages both global and local features by coupling an Attention-Guided DeepLabV3+ backbone with a Multi-Scale Regression Head. A novel feature-injection mechanism enables global grading priors to be fed back into the segmentation decoder, thereby systematically correcting area estimation biases. Second, recognizing the instability of end-to-end optimization, we develop a decoupled training strategy consisting of a pretrain-freeze-finetune procedure designed to mitigate gradient interference between tasks. Third, to address the limited availability of pixel-level annotations, we incorporate a range-based loss function that converts discrete clinical grades into continuous interval constraints, allowing extensive weakly labeled datasets to be effectively exploited in a semi-supervised learning paradigm.

II. RELATED WORK & MOTIVATION ANALYSIS

This section reviews related techniques in embryo grading and, through preliminary experimental data from this study, analyzes the limitations of traditional methods and existing deep learning strategies. This analysis establishes the necessity of adopting the multi-task learning and decoupling strategy proposed in this study.

A. Limitations of Hand-crafted Features

Historically, texture analysis was the primary method for quantifying embryo quality. Since fragmentation manifests primarily as textural anomalies disrupting cytoplasmic uniformity, verifying the efficacy of classic descriptors—specifically the Gray-Level Co-occurrence Matrix (GLCM)—is a necessary prerequisite to justify the transition to deep learning.

1) Data Selection and Clinical Relevance: To ensure the high clinical relevance of our experimental results, all preliminary experiments in this section specifically focus on the Early Cleavage Stage, using embryo images at the T2 (2-cell) and T4 (4-cell) stages. This selection is based on two reasons: First, literature indicates that the degree of fragmentation during the cleavage stage (Day 2-3) is a key early biomarker for predicting whether an embryo can successfully develop to the blastocyst stage [7], [8]. Second, compared to compacted morulae, the cell boundaries and fragment structures at the T2/T4 stages are relatively distinct, making them an ideal scenario for verifying whether algorithms can effectively distinguish between cytoplasmic noise and true fragments.

2) Feature Space Overlap (GLCM Analysis): Based on the T2/T4 dataset, we extracted GLCM texture features from the region of interest (ROI) of embryos and visualized them using t-SNE dimensionality reduction. (As shown in Fig. 1),, even samples with the most disparate grades (Grade A vs. Grade D) exhibit severe overlap in the feature space. This indicates that GLCM features lack sufficient discriminability to overcome common background noise in T2/T4 embryo images, such as cytoplasmic granules and vacuoles, failing to form clear decision boundaries.

3) Failure of Non-linear Mapping: Given the inadequacy of GLCM, we extended our evaluation to Local Binary Patterns (LBP) [9] features, which are more sensitive to local

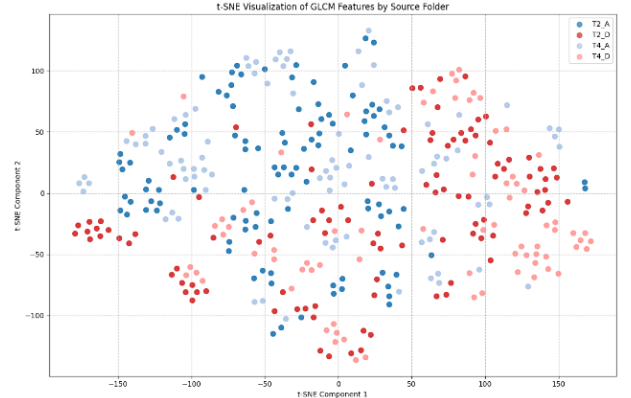


Fig. 1. t-SNE visualization of GLCM texture features.

details, and trained a Multi-Layer Perceptron (MLP) for non-linear regression. Although the model could identify samples with extreme fragmentation (Grade D), it failed to discriminate the subtle differences between intermediate grades (Grade A, B, and C), as illustrated in Fig. 2. This experiment confirms the fundamental deficiency of hand-crafted features in capturing subtle morphological changes in early embryos, establishing the necessity of shifting to End-to-End Deep Learning.

B. Analysis of Deep Learning Baselines

After determining the necessity of deep learning, we evaluated two common automated strategies and identified their respective structural flaws.

1) Pure Regression Models: In our preliminary study, we employed standard CNN architectures (e.g., InceptionV3) to train pure regression models for directly predicting fragmentation ratios. Experimental results demonstrated effective convergence, confirming the capability of CNNs to extract relevant grading features from embryo images. (As shown in Fig. 3), the distribution of the model's predicted values aligns well with the ground truth trends, validating the numerical feasibility of end-to-end grading.

However, this approach suffers from a fundamental clinical flaw: the black-box nature of deep learning. The model outputs only a numerical score without providing any visual evidence of fragment locations. Our analysis revealed that due to the lack of pixel-level supervision, the model frequently attended to non-fragment background noise. This absence of Visual Verification prevents clinicians from

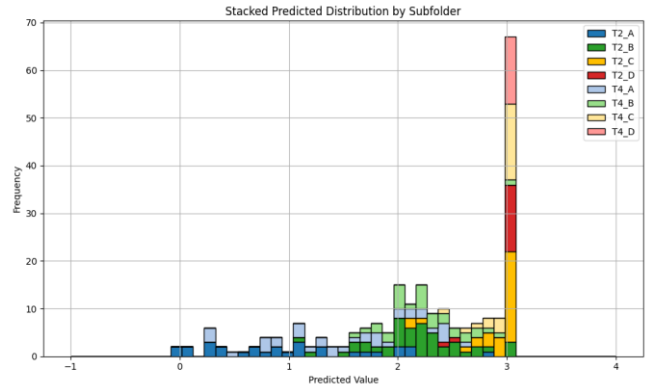


Fig. 2. Prediction distribution of LBP-based MLP model.

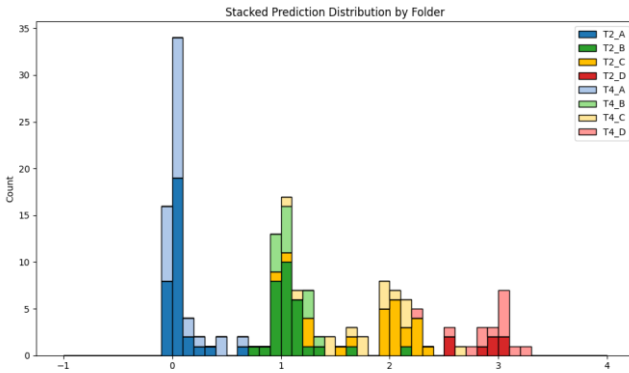


Fig. 3. distribution of predicted clinical grades by the pure regression baseline (inceptionv3).

validating the basis of the grading, thereby failing to meet the strict requirements for Explainability essential in medical AI.

2) *Pure Segmentation Models*: Accumulated Errors in Indirect Grading To address the black box issue, another mainstream approach is to employ semantic segmentation (e.g., DeepLabV3+) to extract fragment regions and calculate the ratio for Indirect Grading.

Core Limitation: Although segmentation models provide excellent explainability, our experiments revealed that grading error (MAE) derived solely from segmentation masks is often limited by uncertainties in mask contour or boundary determination. Embryo fragment boundaries are typically blurred and irregular; minor pixel-level errors generated by the segmentation model during boundary processing can accumulate into significant grading deviations upon integration. This indicates that optimizing the segmentation loss (L_{seg}) alone is insufficient to guarantee the precision of numerical grading.

C. Necessity of Multi-Task Learning and Gradient Conflict

Based on the above analysis, an ideal system must combine the strengths of both approaches: simultaneously outputting precise numerical grading and pixel-level segmentation masks. This motivation aligns with the emerging paradigm of Multi-Task Learning (MTL) in medical imaging [10].

However, MTL is not directly applicable to this task. Research indicates that when there is a competitive relationship between tasks (e.g., the segmentation task pursues high-frequency boundary details, while the regression task pursues low-frequency global abstractions), the shared backbone network faces Gradient Conflict [5], [6]. Specifically, the segmentation gradient L_{seg} tends to optimize for spatial details, whereas the regression gradient L_{reg} tends to optimize for global abstraction. These asymmetric gradient signals can easily induce Negative Transfer in the shared backbone, where the feature representation for segmentation is compromised to optimize regression.

This is the core entry point of this study, driving us to develop the Feature Injection mechanism and the Two-Stage Decoupling strategy.

D. Continuous Handling of Discrete Grades

Clinically, grades A, B, C, and D essentially represent intervals of continuous proportions (0-100%) [11]. Treating this directly as a classification problem results in a loss of magnitude information. Therefore, this study defines the

grading task as Continuous Ratio Regression and utilizes discrete labels to establish Interval Constraints. This approach aligns better with physical reality and provides stable convergence, serving as the theoretical basis for our proposed Range Loss L_{range} .

III. METHODOLOGIES

This section details our proposed AttnRegDeepLab framework. Addressing the gradient conflict and lack of explainability in embryo fragmentation grading, we designed a dual-branch architecture combining Attention-Guided DeepLabV3+ with a Multi-Scale Regression Head, and proposed a Feature Injection mechanism alongside a two-stage decoupled training strategy.

A. System Architecture Design

As shown in Fig. 4, the proposed AttnRegDeepLab framework integrates a shared backbone with two task-specific branches: a regression subsystem for global quantification and an attention-guided segmentation subsystem for local boundary delineation.

1) *Shared Backbone and Multi-Scale Features*. We adopt ResNet-50 as the shared feature extractor. To accommodate the spatial resolution requirements of semantic segmentation, we modified the standard architecture by removing the downsampling stride in Layer 3 and Layer 4. Instead, we employed dilated convolutions, with rate values of 2 and 4 at layer 3 and layer 4, respectively, to maintain the output stride of the final feature map (F_4) at 8. This modification allows the backbone to preserve high-level semantic abstraction without losing essential spatial details. The model extracts

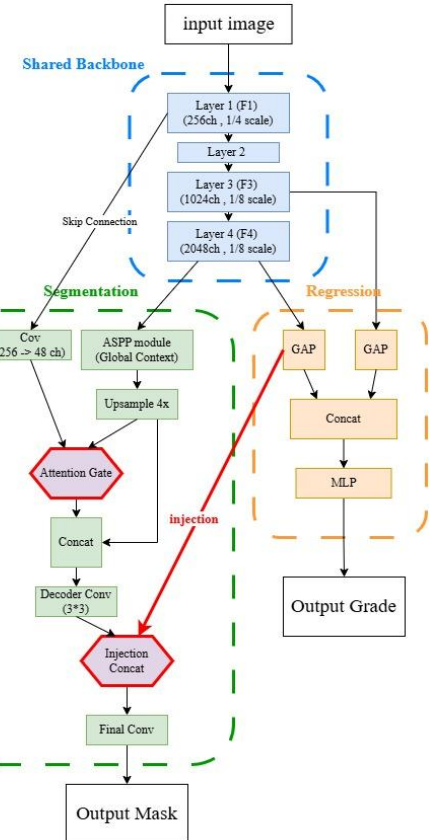


Fig. 4. Schematic overview of AttnRegDeepLab. The framework comprises a shared ResNet-50 backbone (blue), an attention-guided segmentation branch (green), and a multi-scale regression branch (orange). The red arrow indicates the U-Net skip connection, while the 'Injection' module represents the feature fusion bridge.

features from multiple levels for downstream tasks, specifically utilizing the low-level F_1 features (Layer 1, 1/4 scale, 256 channels) for boundary recovery, and the high-level F_3 (Layer 3, 1024 channels) and F_4 (Layer 4, 2048 channels) features as the core inputs for segmentation context and regression analysis.

2) *Regression Subsystem*: To map input images to a continuous grading scale $\hat{y}_{\text{reg}} \in [0, 1]$, we designed a Multi-Scale Regression Head. Deep features from layers F_3 and F_4 are fused and processed via Global Average Pooling (GAP) followed by a Multi-Layer Perceptron (MLP). Crucially, we extract a latent feature vector $V_{\text{reg}} \in \mathbb{R}^{2048}$ from the penultimate layer of the MLP. This vector serves as a compact representation of global fragmentation severity, which is subsequently injected into the segmentation branch to guide pixel-level predictions.

3) *Attention-Guided Segmentation Subsystem*: To overcome the over-smoothing inherent in standard DeepLabV3+ and correct systematic area estimation errors, we redesigned the decoder into a three-stage refinement pipeline:

Multi-Scale Context Extraction: First, the deep backbone features (F_4) are processed through an Atrous Spatial Pyramid Pooling (ASPP) module. This captures multi-scale contextual information, yielding a high-level semantic map F_{ASPP} .

Attention-Guided Boundary Refinement: To recover fine spatial details lost during down-sampling without introducing cytoplasmic noise, we replaced the standard skip connection with an Attention Gate (AG). Let $F_1 \in \mathbb{R}^{C_1 \times H \times W}$ denote the shallow features from the backbone and $g = \text{Up}(F_{\text{ASPP}})$ be the upsampled gating signal. The attention coefficient map α is formulated in (1):

$$\alpha = \sigma \left(\psi \left(\text{ReLU}(W_x(F_1) + W_g(g) + b) \right) \right). \quad (1)$$

The refined shallow features are then obtained by $\hat{F}_1 = \alpha \odot F_1$. This mechanism effectively filters out background texture noise before concatenation with the deep features.

Regression-Guided Feature Injection: Finally, to align the pixel-level segmentation with the global severity grade, we introduce a Feature Injection mechanism at the end of the decoder. The global regression vector V_{reg} is spatially broadcasted and fused with the decoder features F_{dec} :

$$F_{\text{inj}} = \text{Broadcast}(V_{\text{reg}}) \in \mathbb{R}^{C_{\text{reg}} \times H \times W}, \quad (2)$$

$$F_{\text{final}} = \text{Concat}(F_{\text{dec}}, F_{\text{inj}}). \quad (3)$$

By conditioning the final convolution on F_{final} , the model incorporates global grading priors to rectify local segmentation ambiguities.

B. Hybrid Loss Function

To coordinate the pixel-level and image-level tasks under semi-supervised settings, we minimize a composite objective:

$$L_{\text{total}} = \alpha L_{\text{seg}} + \beta L_{\text{reg}} + \gamma L_{\text{cons}}. \quad (4)$$

1) *Segmentation Loss (L_{seg})*: To address class imbalance between sparse fragments and the background, L_{seg} is defined as the weighted sum of Binary Cross Entropy, Dice Loss [12], and Focal Loss.

2) *Regression Loss (L_{reg})*: We adopt a dual-strategy. For samples possessing complete pixel-level supervision (referred to here as paired data, D_{paired}), we employ a precise regression loss (denoted as L_{pre}), calculates the L1 error against the ground truth ratio derived from pixel-level annotations. Conversely, for samples limited to clinical grades only (D_{weak}), consistent with emerging weak supervision paradigms in medical imaging [13], we propose a Range Loss (L_{range}). Mapping each discrete grade G to a continuous interval $[y_{\text{min}}, y_{\text{max}}]$, the loss penalizes predictions \hat{y} only when they violate interval bounds:

$$L_{\text{range}}(\hat{y}, G) = \text{ReLU}(y_{\text{min}} - \hat{y}) + \text{ReLU}(\hat{y} - y_{\text{max}}). \quad (5)$$

This formulation enables the utilization of large-scale clinical records without enforcing arbitrary point-labels.

3) *Consistency Loss (L_{cons})*: To enforce logical consistency, we minimize the discrepancy between the regression prediction and the area ratio derived from the segmentation mask, ensuring that geometrical and numerical outputs are mutually reinforcing.

C. Two-Stage Decoupled Training Strategy

Addressing the Negative Transfer phenomenon common in multi-task learning, where competing gradients destabilize the shared backbone, we propose a temporally decoupled training strategy.

In Phase 1 (Visual Expert Pre-training), the objective is to train the backbone network's ability to extract spatial features and optimize boundaries using the Attention mechanism. In this phase, we enable only L_{seg} and L_{cons} ($\beta=0$) and initialize the model with ImageNet weights. This results in a feature extractor with optimal visual fidelity, establishing a baseline for instance segmentation.

In Phase 2 (Regression-Guided Finetuning), we address the gradient conflict. We freeze the parameters of the shared backbone θ_{backbone} learned in Phase 1, treating it as a fixed feature extractor. Optimization is restricted to the regression head θ_{reg} and the feature injection layers..

$$\theta_{\text{backbone}}^{(t+1)} = \theta_{\text{backbone}}^{(t)} \quad (\text{Frozen}). \quad (6)$$

This strategy prevents the regression gradients—which prioritize global quantity—from disrupting the high-frequency spatial features essential for segmentation boundaries, effectively isolating the negative transfer phenomenon.

IV. EXPERIMENTAL RESULTS

To verify the effectiveness of the proposed AttnRegDeepLab framework, rigorous ablation studies were conducted to quantify the gradient trade-off between segmentation and regression tasks. We first describe the experimental setup, followed by a step-by-step analysis of component removal to evaluate the specific impact of the Feature Injection mechanism and the Two-Stage Decoupled strategy on model performance.

A. Experimental Setup

1) *Data Source and Partitioning*: This study utilizes clinical embryo images focused on the critical cleavage stage (2-cell and 4-cell). To evaluate the efficacy of semi-supervised learning, the dataset was split into two subsets.

First, Paired Data (D_{paired}) with 318 samples annotated with both pixel-level fragmentation masks and clinical grades. This subset supports fully supervised training for segmentation (L_{seg}) and precise regression (L_{pre}). Secondly, Grade-Only Data (D_{weak}) of 1549 samples annotated with clinical grades without segmentation masks. This subset is utilized exclusively for weakly supervised regression via the proposed Range Loss (L_{range}).

2) *Preprocessing*: To prevent geometric distortion during feature extraction, all input images were preprocessed using an aspect-ratio preserving resize strategy with zero-padding, standardizing the resolution to 299×299 pixels.

3) *Implementation Details*: The framework was implemented using PyTorch. Optimization was performed using the AdamW optimizer. To manage the stability of the decoupled training strategy, we adopted a differential learning rate schedule: a base learning rate of 1×10^{-4} was used for the Unfrozen (Full MTL) phase to learn global features, while a reduced rate of 1×10^{-5} was applied during the Frozen (Decoupled) finetuning phase to preserve the pre-trained feature space. All experiments were conducted on an NVIDIA RTX 3060 GPU.

4) *Evaluation Metrics*: Performance was assessed using two primary metrics. (1) Dice Similarity Coefficient (DSC): Measures the spatial overlap between the predicted segmentation mask and the expert annotation, quantifying shape fidelity. Mean Absolute Error (MAE): Evaluates the accuracy of the regression head in predicting the fragmentation ratio against the ground truth clinical assessment.

B. Preliminary Study: Architecture Selection and Verification

Before investigating multi-task training strategies, we first validated the necessity of the proposed AttnRegDeepLab segmentation backbone. To confirm the benefits of integrating Attention Gates into the U-Net skip connections, we compared our architecture against the Standard DeepLabV3+ baseline in a single-task setting. Experimental results (summarized in Table 4.2, Rows 1-2) indicate that while the Standard DeepLabV3+ benefits from the ASPP module for global semantics, its segmentation accuracy stagnates at Dice=0.717. Qualitative analysis reveals a tendency towards over-smoothing and misclassification of cytoplasmic granules near blurred fragment boundaries. In contrast, by incorporating attention-guided shallow features (F_1), our proposed method successfully elevates the segmentation accuracy to 0.729 (+1.2%). This empirical evidence confirms that filtering high-frequency noise via Attention Gates is critical for improving boundary discriminability in embryo fragmentation. This experiment establishes AttnRegDeepLab (Exp A) as a robust visual baseline for subsequent multi-task experiments.

C. Ablation Study and Core Analysis

A series of ablation experiments are conducted to systematically quantify the gradient trade-off in multi-task learning and verify the efficacy of the proposed feature injection and decoupling strategies.

1) *Experiment settings*: To systematically isolate the contribution of each component and verify our hypotheses,

we defined five controlled configurations alongside the Standard DeepLabV3+ Baseline (summarized in Table 1):

Exp A (Visual Baseline/S1): Uses the AttnRegDeepLab segmentation branch trained independently with optimization restricted to segmentation objectives ($L_{\text{seg}} + L_{\text{cons}}, \beta = 0$). This setup aims to establish the theoretical upper bound for segmentation accuracy (S1) without interference from regression gradients.

Exp B (Regression Baselines): Consists of pure regression models to benchmark quantification accuracy in the absence of spatial supervision. To validate the efficacy of the proposed Range Loss, we stratify this into Exp B1 (Paired Only), trained exclusively on the D_{paired} subset, and Exp B2 (Semi-supervised), trained on the full dataset ($D_{\text{paired}} + D_{\text{weak}}$). Comparing B1 and B2 allows us to quantify the explicit benefit of incorporating weakly labeled data prior to integrating it into the full multi-task framework.

Exp C (Full MTL): Implements the complete End-to-End AttnRegDeepLab with Feature Injection, where all loss components are active (L_{total}). This experiment is designed to analyze the Shape-Area Trade-off under joint optimization and assess the impact of gradient conflict.

Exp D (Decoupled Strategy): Adopts the proposed Pretrain-Freeze-Finetune strategy. By optimizing L_{seg} in Phase 1 and L_{reg} in Phase 2 (with a frozen backbone), this experiment verifies the hypothesis of positive transfer, testing whether fixed spatial features can support accurate regression without catastrophic forgetting.

Exp E (No-Inject Control): Serves as a strict ablation control for Exp C where the Feature Injection mechanism is disconnected, while maintaining the same joint loss function (L_{total}). Comparing Exp C and Exp E allows us to isolate the specific contribution of the physical feature bridge in coordinating the two tasks. The quantitative results of these experiments are summarized in Table 1.

Table 1: Quantitative Results of Ablation Study

Exp ID	Architecture & Strategy	Strategy	Loss Setting	Dice Score (F1)	MAE (Direct)
Baseline	Vanilla DeepLabV3+	Single Task	$L_{\text{seg}} + L_{\text{cons}}$	0.717	N/A
Exp A	AttnRegDeepLab	Single Task	$L_{\text{seg}} + L_{\text{cons}}$	0.729	N/A
Exp B1	Pure Regression	Single Task	L_{pre}	N/A	0.057
Exp B2	Pure Regression	Single Task	$L_{\text{reg}} (L_{\text{pre}} + L_{\text{range}})$	N/A	0.051
Exp C	AttnRegDeepLab	Full MTL	L_{total}	0.716	0.046
Exp D	AttnRegDeepLab	Decoupled	Phase 1: L_{seg} Phase 2: L_{reg}	0.729	0.049
Exp E	AttnRegDeepLab (No-Inject)	Full MTL	L_{total}	0.678	0.053

2) Quantitative Analysis.

As listed in Table 1, the experimental results validate our core hypotheses regarding feature interaction and gradient dynamics.

Validation of Feature Injection Mechanism (Exp C vs. Exp E): To verify whether Feature Injection is the catalyst for multi-task success, we compared Exp C (With Injection) against Exp E (No Injection/Disconnected). The *results indicate that under the exact same full training strategy*, removing the injection mechanism caused significant performance degradation. Specifically, the segmentation Dice dropped from 0.716 to 0.678, and grading MAE worsened from 0.046 to 0.053—performing even worse than the single-task baseline. This provides strong evidence that simply summing segmentation and regression losses leads to destructive gradient conflict. Only through the Feature Injection mechanism—which physically guides the segmentation decoder with global semantic features extracted by the regression head—can the optimization directions of these two tasks be coordinated, transforming conflict into mutual assistance.

Efficacy of Weak Labels (Exp B1 vs. Exp B2): Prior to evaluating the multi-task framework, we verified the contribution of the proposed Range Loss using the regression baselines. As shown in Table 1, training solely on limited paired data (Exp B1, N=318) resulted in a higher grading error (MAE = 0.057). However, by incorporating the large-scale grade-only dataset via interval constraints (Exp B2, N=1549), the error significantly decreased to 0.051. This improvement confirms that the Range Loss successfully extracts valuable global priors from discrete clinical grades, mitigating the data scarcity problem and justifying its application in the subsequent multi-task experiments (Exp C/D).

Gradient Trade-off and Optimal Grading: The results of Exp C revealed a significant Shape-Area Trade-off in deep learning optimization. To accommodate the regression task's strict requirement for total quantity accuracy, the backbone network sacrificed high-frequency boundary details, resulting in a slight decrease in Dice from the S1 baseline (0.729) to 0.716. However, the cost of this global optimization yielded the best precision for the regression head (MAE=0.046), outperforming the pure regression baseline (0.051) and matching the accuracy of segmentation-derived grading. This is qualitatively corroborated in Fig. 5; while the S1 Model (Exp A) produces sharper boundaries around small fragments (Column 3), the Full MTL Model (Exp C) generates slightly smoother masks (Column 4). Nevertheless, Exp C's global area estimation aligns more consistently with the ground truth grading. This indicates that if the primary clinical goal is precise numerical grading, the end-to-end feature injection strategy is the optimal choice.

Robustness of the Decoupled Strategy: In terms of addressing the high clinical standards for both explainability and model stability, Exp D (Frozen Finetuning) offers the most balanced solution. Although its MAE (0.049) is marginally inferior to Exp C, it perfectly preserves the SOTA segmentation accuracy of Exp A (Dice 0.729), effectively insulating the visual features from regression gradient

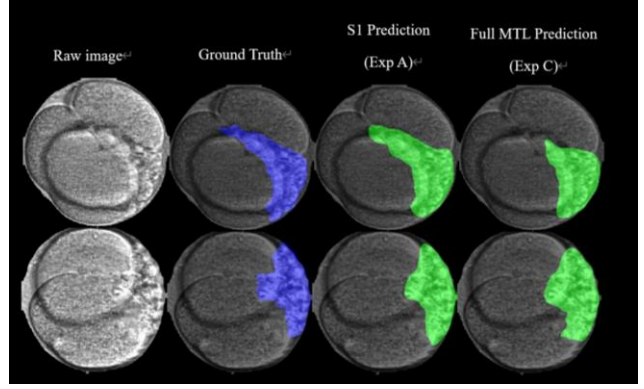


Fig. 5. Qualitative Comparison of Segmentation Results. Columns from left to right: (a) Raw input image. (b) Ground Truth (Blue). (c) Prediction from S1 Model (Exp A) showing sharp boundaries (Green). (d) Prediction from Full MTL Model (Exp C) showing slight over-smoothing but consistent area estimation.

interference. This proves that the spatial features learned in Phase 1 possess strong generalization capabilities and can be directly utilized by the regression head for positive transfer, making Exp D the most robust candidate for clinical deployment.

Synthesizing the above findings, this study confirms that it is difficult for a single model to optimize pixel-level accuracy (DICE coefficient) and visual conformity (MAE). Therefore, we propose a Task-Specific Dual-Module Deployment Strategy deployment strategy as the optimal clinical solution: utilizing the S1 Model (Exp A) to provide the highest fidelity visual aid (XAI), while simultaneously using the Full MTL Model (Exp C) to provide the lowest error automated grading. This solution not only surpasses traditional methods and single-task baselines in technical metrics but also offers a flexible and trustworthy choice for clinical utility..

V. CONCLUSION

We have presented a multi-task learning framework AttnRegDeepLab capable of addressing the challenges of subjectivity and lack of interpretability in embryo fragmentation grading. Unlike traditional approaches that treat grading as black-box regression or discrete classification, we recast the task into a continuous quantification problem with pixel-level explainability. We have shown the incapability of traditional hand-crafted features (GLCM/LBP) for this specific task, which motivated us toward a semantic segmentation-based paradigm. To mitigate the gradient conflict inherent in multi-task learning, we subsequently designed a Feature Injection mechanism and a Two-Stage Decoupled training strategy. Through rigorous ablation studies, we successfully quantified the trade-off between segmentation precision and grading accuracy, ultimately proposing a clinically deployable solution.

Key findings of this study include: (1) Necessity of Architecture Upgrade in Experiment A that confirmed that introducing Attention Gates and U-Net Skip Connections effectively filters cytoplasmic noise in shallow features, elevating segmentation accuracy from the standard DeepLabV3+ baseline of 0.717 to 0.729 (SOTA). This establishes a foundation for high-fidelity visual explanation. (2) Effectiveness of Feature Injection Mechanism: Comparing by Exp C (With Injection) and Exp E (No Injection) that indicated, by removing the injection mechanism, the grading

error could significantly worsen from 0.046 to 0.053. This shows that multi-task loss functions alone are insufficient to coordinate task conflicts; physical feature concatenation is required to guide the segmentation decoder with global grading semantics to achieve positive transfer. (3) Existence of Gradient Trade-off by Exp C to reveal an intrinsic trade-off between pixel-level precision and the image-level accuracy. To reduce the grading error MAE to as low as 0.046, the model sacrificed some edge segmentation details (Dice 0.716), verifying that a single model cannot satisfy the two goals simultaneously.

In short, the proposed method can provide a visual assistant (Exp A/S1) to deliver superior segmentation fidelity with Dice value 0.729. This function can assist embryologists in rapid anomaly localization and morphological verification, providing clear visual evidence of fragmentation patterns. In addition, our method can also provide automated quantification (Exp C/Full MTL) to achieve regression error MAE as low as 0.046. This serves as an objective benchmark to mitigate inter-observer variability, ensuring consistent grading across different operators.

The limitation of this study lies in the use of static images from a single time point. Future research directions will integrate Time-lapse images to extend AttnRegDeepLab to a spatiotemporal model, or we may try the use of a transformer-based approach, exploring the impact of dynamic fragmentation processes on embryo developmental potential.

REFERENCES

- [1] T. Ebner et al., "Selection based on morphological assessment of oocytes and embryos at different stages of preimplantation development: a review," *Human Reproduction Update*, vol. 9, no. 3, pp. 251–262, 2003.
- [2] M. Alikani, A. Cohen, J. Tomkin, G. J. Garrisi, C. Mack, and R. T. Scott, "Human embryo fragmentation in vitro and its implications for pregnancy and implantation," *Fertility and Sterility*, vol. 71, no. 5, pp. 836–842, 1999.
- [3] I. Paternot et al., "Intra- and inter-observer analysis in the morphological assessment of human embryos," *Reproductive BioMedicine Online*, vol. 19, no. 6, pp. 836–844, 2009.
- [4] A. Sundvall et al., "Inter-observer variability in the assessment of day 3 embryo quality: a multinational study," *Human Reproduction*, vol. 28, no. 1, pp. 71–77, 2013.
- [5] T. Standley et al., "Which tasks should be learned together in multi-task learning?", in *Proc. Int. Conf. Mach. Learn. (ICML)*, 2020, pp. 9120–9132.
- [6] T. Yu, S. Kumar, A. Gupta, S. Levine, K. Hausman, and C. Finn, "Gradient surgery for multi-task learning," in *Adv. Neural Inf. Process. Syst. (NeurIPS)*, 2020.
- [7] M. Alikani et al., "Cleavage anomalies in early human embryos and survival after prolonged culture in-vitro," *Human Reproduction*, vol. 15, no. 12, pp. 2634–2643, 2000.
- [8] C. Racowsky et al., "The effect of assessing early embryo cleavage status on blastocyst development," *Fertility and Sterility*, vol. 74, no. 5, pp. 900–905, 2000.
- [9] T. Ojala, M. Pietikainen, and T. Maenpaa, "Multiresolution gray-scale and rotation invariant texture classification with local binary patterns," *IEEE Trans. Pattern Anal. Mach. Intell.*, vol. 24, no. 7, pp. 971–987, 2002.
- [10] H. Ben Cohen et al., "Multi-task deep learning for simultaneous classification and segmentation of cancer pathologies in diverse medical imaging modalities," *Cancers*, vol. 16, no. 3, p. 34, 2024.
- [11] Alpha Scientists in Reproductive Medicine and ESHRE Special Interest Group of Embryology, "The Istanbul consensus workshop on embryo assessment: proceedings of an expert meeting," *Human Reproduction*, vol. 26, no. 6, pp. 1270–1283, 2011.
- [12] F. Milletari, N. Navab, and S.-A. Ahmadi, "V-Net: Fully convolutional neural networks for volumetric medical image segmentation," in *Proc. 3D Vis. (3DV)*, 2016, pp. 565–571.
- [13] N. H. Shah et al., "Weakly supervised deep learning in radiology," *Radiology*, vol. 312, no. 1, p. e232085, Jul. 2024.